Experimental Validation of a Novel Gauss-Newton Inversion Method for Microwave Tomographic Imaging

Alessandro Fedeli[1], Matteo Pastorino[1], and Andrea Randazzo[1]*

[1]Department of Electrical, Electronic, Telecommunications Engineering, and Naval Architecture
University of Genoa
Via Opera Pia 11A, I-16145 Genoa, Italy
e-mail: alessandro.fedeli@edu.unige.it; matteo.pastorino@unige.it; andrea.randazzo@unige.it

Abstract

Microwave imaging systems are acquiring an ever growing importance. In order to tackle the nonlinearity and ill-posedness of the underlying inverse scattering problems, several inversion approaches have been formulated in the scientific community. In this framework, an efficient Gauss-Newton method, based on a regularization in Banach spaces, has been recently developed and numerically tested. In this paper, an experimental validation of the approach using real data is provided.

1. Introduction

In recent years, there has been a growing interest in the development of microwave imaging systems [1]–[6]. In fact, such systems are in principle able to directly provide the distributions of some of the physical properties of the unknown targets under test (e.g., the dielectric permittivity and the electric conductivity) starting from measurements of the electric field scattered by a given target when illuminated by incident waves at microwave frequencies. An example of these systems is represented by the prototype described in [7], which is intended for applications in the wood industry.
As it is well known, the electromagnetic inverse scattering problem (which represents the basic mathematical formulation of microwave imaging systems) turns out to be non-linear and strongly ill-posed. Consequently, developing efficient methods able to obtain meaningful reconstructions is not an easy task. In particular, it is necessary to devise specifically designed inversion schemes, incorporating nonlinear regularization techniques.

Several methods have been proposed in the past, employing both deterministic and stochastic strategies [8]–[13]. Among the others, the present Authors recently developed an efficient inexact-Newton inversion method in [14], [15]. In most cases, regularization methods are exploited in the context of Hilbert spaces. Although being very powerful, such approaches usually give rise to smooth (and sometimes over-smooth) reconstructions, often characterized by artifacts and ripples. An imaging approach based on a Gauss-Newton strategy combined with a regularization working in Banach spaces (i.e., complete vector spaces endowed with a norm that only allows "length" and "distances" between its elements to be measured) has been introduced in [16]. Due to the geometrical properties of Banach spaces, this method allows to obtain solutions with lower over-smoothness and less artifacts than standard Hilbert-space ones. This new approach has been numerically tested in [17], [18]. In this paper, a validation of the proposed method by using real scattering data experimentally measured is reported and discussed.

The present contribution is organized as follows. The mathematical formulation of the approach is briefly recalled in Section 2. Some examples of the results provided by the developed inversion procedure are described in Section 3. Finally, conclusions are drawn in Section 4.

2. Mathematical Formulation

Let us consider a tomographic imaging configuration. The target is modeled as an infinite cylinder with axis parallel to z direction, whose cross-section is located within an investigation domain D_{inv}. A transmitting antenna generating a TM-polarized electromagnetic field at microwave frequencies is used to illuminate the investigated region. Moreover, the scattered electric field is measured in an observation domain D_{meas}. A $e^{j\omega t}$ time dependence is assumed and omitted in the following. As it is well known, for this configuration the scattering problem turns out to be scalar and two-dimensional [1]. The z-component of the scattered electric field E_{scatt} originated by the presence of the object is given by

$$E_{scatt}(\mathbf{r}) = \mathcal{G}_{data}(\chi E_{tot})(\mathbf{r}) = -k^2 \int_{D_{inv}} \chi(\mathbf{r}') E_{tot}(\mathbf{r}') g(\mathbf{r}, \mathbf{r}') d\mathbf{r}' , \qquad \mathbf{r} \in D_{meas} , \tag{1}$$

978-1-4673-5225-3/14/$31.00 ©2014 IEEE

where E_{tot} is the z-component of the total electric field, $k = \omega\sqrt{\varepsilon_0\mu_0}$ is the vacuum wavenumber (being ε_0 the dielectric permittivity and μ_0 the magnetic permeability of the vacuum), $g(\mathbf{r},\mathbf{r}') = jH_0^{(2)}(k|\mathbf{r}-\mathbf{r}'|)/4$ is the 2D Green function for the present scattering configuration (being $H_0^{(2)}$ the Hankel function of zeroth order and second kind), and χ is the contrast function, defined as

$$\chi(\mathbf{r}) = \varepsilon_r(\mathbf{r}) - 1 - j\frac{\sigma(\mathbf{r})}{\omega\varepsilon_0}, \qquad \mathbf{r} \in D_{inv}\,. \tag{2}$$

where ε_r and σ are the relative dielectric permittivity and the electric conductivity of the investigation domain D_{inv}. Since the total electric field inside the investigation domain is unknown, a second equation is necessary in order to find a solution of the electromagnetic problem, i.e.,

$$E_{tot}(\mathbf{r}) = E_{inc}(\mathbf{r}) + \mathcal{G}_{state}(\chi E_{tot})(\mathbf{r}) = E_{inc}(\mathbf{r}) - k^2 \int_{D_{inv}} \chi(\mathbf{r}')E_{tot}(\mathbf{r}')g(\mathbf{r},\mathbf{r}')d\mathbf{r}', \qquad \mathbf{r} \in D_{inv}\,. \tag{3}$$

Equation (1) and equation (3) can be joined together so as to obtain the following non-linear scattering equation

$$E_{scatt}(\mathbf{r}) = \mathcal{F}(\chi)(\mathbf{r}), \qquad \mathbf{r} \in D_{meas}\,, \tag{4}$$

where $\mathcal{F}: X \to Y$ is a non-linear operator that maps the contrast function $\chi \in X$ into the scattered field $\mathcal{F}(\chi) \in Y$. Equation (4) is solved by means of an iterative approach which searches for a minimum of the functional $\Phi: X \to \mathbb{R}$

$$\Phi(\chi) = \frac{1}{2}\|\mathcal{F}(\chi)(\mathbf{r}) - E_{scatt}(\mathbf{r})\|_Y^2, \qquad \mathbf{r} \in D_{meas} \tag{5}$$

by accomplishing a regularization in the L^p spaces of p-summable functions, with $1 < p < +\infty$ ($X = Y = L^p$). The algorithm is essentially composed by two nested cycles: an outer cycle for performing a Gauss-Newton linearization of the operator $\mathcal{F}$ around to the current reconstructed contrast function, and an inner cycle, which solves the linearized equation applying a truncated Landweber regularization scheme in Banach spaces. Furthermore, our algorithm is able to exploit the information gathered from scattered field data acquired at F different frequencies f_i ($E_{scatt}^{(i)}, i = 1,..,F$) by using a frequency-hopping approach. In details, the algorithm works as follows (i is the frequency index, n is the outer index, and l the inner one):

A. Initialize the inversion algorithm at the ith frequency. The outer iteration index is set to $n = 0$ and the starting guess $\chi_0^{(i)} \in X$ is initialized with

$$\chi_0^{(i)} = \begin{cases} 0, & i = 1 \\ \hat{\chi}^{(i-1)}, & 1 < i \le F \end{cases} \tag{6}$$

1. Linearize the operator $\mathcal{F}$ around $\chi_n^{(i)}$, in order to obtain the linear equation

$$\mathcal{F}_{\chi_n^{(i)}} h_n^{(i)} = E_n^{(i)}\,. \tag{7}$$

The operator $\mathcal{F}_{\chi_n^{(i)}}: X \to Y$ is the Frèchet derivative of $\mathcal{F}$ at $\chi_n^{(i)} \in X$ and $E_n^{(i)} = E_{scatt}^{(i)} - \mathcal{F}\left(\chi_n^{(i)}\right) \in Y$.

2. Solve equation (7) by using the Landweber regularization algorithm in Banach spaces (inner loop)

$$\begin{gathered} h_{n,0}^{(i)} = \tilde{h}_{n,0}^{(i)} = 0 \\ \begin{cases} \tilde{h}_{n,l+1}^{(i)} = \tilde{h}_{n,l}^{(i)} - \tau\mathcal{F}_{\chi_n^{(i)}}^{*} J^{Y}\left(\mathcal{F}_{\chi_n^{(i)}} h_{n,l}^{(i)} - E_n^{(i)}\right) \\ h_{n,l+1}^{(i)} = J^{X^*}\left(\tilde{h}_{n,l+1}^{(i)}\right) \end{cases}, \; l = 0,1,2,\ldots \end{gathered} \tag{8}$$

being $\mathcal{F}_{\chi_n^{(i)}}^{*}: Y^* \to X^*$ the adjoint operator of $\mathcal{F}_{\chi_n^{(i)}}$ and $\tau > 0$ the step length. The operators J^Y and J^{X^*} are the duality maps of the Banach spaces Y and X^* [16]. In L^p spaces, they are defined as $J^{L^p}(\cdot) = \|\cdot\|_{L^p}^{2-p}|\cdot|^{p-1}\mathrm{sign}(\cdot)$, where $\mathrm{sign}(s) = e^{j\arg(s)}$ if $s \neq 0$ and 0 otherwise. These inner steps are iterated until an a-priori convergence criterion is satisfied (at iteration $l = l_{opt}$). Then, the regularized solution is denoted as $\hat{h}_n^{(i)} = h_{n,l_{opt}}^{(i)}$.

3. Update the current solution with $\chi_{n+1}^{(i)} = \chi_n^{(i)} + \hat{h}_n^{(i)}$.

4. The outer steps 1-3 are iterated until some a-priori convergence criterion is fulfilled (at iteration $n = n_{opt}$). Then, the outer cycle is terminated and $\hat{\chi}^{(i)} = \chi_{n_{opt}}^{(i)}$ is the solution at frequency index i.

B. Update the frequency index and iterate from A, until all the frequencies f_i, $i = 1, .., F$, are processed.

3. Experimental Results

In this work, an experimental validation of the developed algorithm is presented. In particular, the results obtained with the *FoamDielIntTM* experimental dataset provided by the Institut Fresnel of Marseille (France) [19] are reported in the following. The target is a combination of two cylinders: the first one is a foam cylinder of diameter $d_1 = 80$ mm with center at the origin and characterized by a relative dielectric permittivity $\varepsilon_{r,1} = 1.45$, whereas the second one is a plastic cylinder of diameter $d_2 = 31$ mm, centered at $(-5; 0)$ mm, and with $\varepsilon_{r,2} = 3$. The target is illuminated from $S = 8$ different directions and the scattered electric field is measured at $M = 241$ locations (additional information about the measurement setup can be found in [19]). Measurements have been taken at $F = 9$ different frequencies (from 2 to 10 GHz with a frequency step of 1 GHz). In the inversion algorithm, D_{inv} has been divided into 40×40 square subdomains. Furthermore, the maximum numbers of outer and inner iterations have been set equal to $n_{max} = 20$ and $l_{max} = 10$, respectively. Moreover, the two nested loops have been stopped when the variation of the residual Φ between two subsequent iterations is below 1%.

The inversion algorithm has been run for different values of the parameter p, which characterizes the working Banach space. For $p = 2$, the approach provides the standard Hilbert space reconstruction. Moreover, the performance of the frequency hopping strategy has also been evaluated by varying the number of considered frequencies, F; in particular, for a fixed value of F, the set of considered frequencies is $f_i = 2 + (i - 1)$ GHz, $i = 1, \dots, F$. The relative reconstruction errors e_{rel} (referred to the whole investigation domain) versus the norm parameter p and for different sets of frequencies are reported in Figure 1. As can be seen, for this case, when considering only a small frequency set, the best results are achieved with low values of p. When using a wider set of frequencies, containing also the higher ones, reconstruction errors are almost constant with respect to p. However, in this case, larger values of p seem to provide slight enhancements in the global reconstruction error. Some of the reconstructed dielectric profiles are shown in Figure 2.

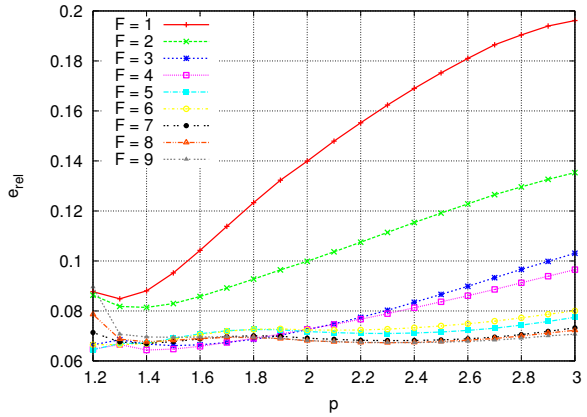

Figure 1. Relative reconstruction errors for the whole investigation domain versus the parameter p and for different numbers of considered frequencies.

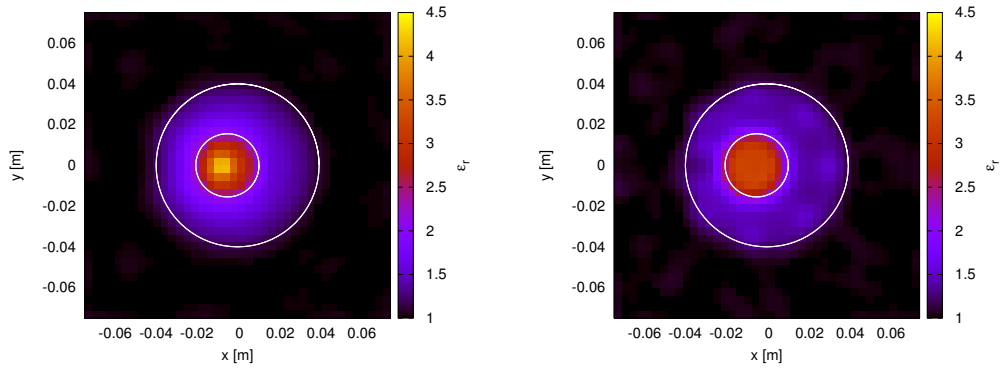

(a) (b)

Figure 2. Reconstructed distribution of the dielectric permittivity for the target FoamDielIntTM: (a) overall best reconstruction ($p = 1.4$, $F = 4$); (b) best reconstruction using all the available data ($p = 2.3$, $F = 9$).

In particular, Figure 2(a) shows the overall best reconstruction, achieved with $p = 1.4$ and considering four frequencies (between 2 GHz and 5 GHz). The object appears to be correctly reconstructed, although the permittivity at the center of the plastic cylinder is slightly overestimated. Figure 2(b) reports the best reconstruction obtained using all the data (with frequencies from 2 to 10 GHz), and is related to the case $p = 2.3$. Clearly, in this case, too, the method is able to correctly reconstruct the target. However, even if the dielectric permittivity of the plastic cylinder is closer to the actual one, several artifacts and ripples are present in the reconstructed image.

4. Conclusions

An experimental validation of a recently proposed approach has been reported in this paper. Such approach is based on a Gauss-Newton strategy incorporating a regularization in L^p Banach spaces, which allows to obtain solutions characterized by a lower over-smoothness and less artifacts than standard Hilbert-space ones. The reported results show that, in the considered case, the new approach provide better results than standard inversion procedure developed in Hilbert spaces, especially when considering a limited set of data. Moreover, as expected, the use of a frequency hopping scheme leads to a significant reduction of the reconstruction errors. Further developments will be devote to evaluate the effectiveness of the approach when applied to some applicative scenarios. In particular, we are interested in preliminary assessing the applicability in the wood industry by using experimental data collected by the prototype of imaging system mentioned in the Introduction.

References

1. M. Pastorino, *Microwave Imaging*, Hoboken N.J.: John Wiley, 2010.
2. R. Marklein, K. Balasubramanian, A. Qing, and K. J. Langenberg, "Linear and nonlinear iterative scalar inversion of multi-frequency multi-bistatic experimental electromagnetic scattering data," *Inverse Probl.*, **17**, December 2001, pp. 1597–1610.
3. Y. Shlivinski and E. Heyman, "Physical Models for Polarimetric SAR Analysis," *IEEE Trans. Antennas Propag.*, **56**, August 2008, pp. 2664–2672.
4. M. Ostadrahimi, P. Mojabi, A. Zakaria, J. LoVetri, and L. Shafai, "Enhancement of Gauss-Newton Inversion Method for Biological Tissue Imaging," *IEEE Trans. Microw. Theory Tech.*, **61**, 2013, pp. 3424–3434.
5. M. T. Ghasr, M. A. Abou-Khousa, S. Kharkovsky, R. Zoughi, and D. Pommerenke, "Portable Real-Time Microwave Camera at 24 GHz," *IEEE Trans. Antennas Propag.*, **60**, 2012, pp. 1114–1125.
6. A. Semnani, I. T. Rekanos, M. Kamyab, and T. G. Papadopoulos, "Two-Dimensional Microwave Imaging Based on Hybrid Scatterer Representation and Differential Evolution," *IEEE Trans. Antennas Propag.*, **58**, October 2010, pp. 3289–3298.
7. A. Salvade, M. Pastorino, R. Monleone, G. Bozza, and A. Randazzo, "A New Microwave Axial Tomograph for the Inspection of Dielectric Materials," *IEEE Trans. Instrum. Meas.*, **58**, July 2009, pp. 2072–2079.
8. R. Ferraye, J.-Y. Dauvignac, and C. Pichot, "An inverse scattering method based on contour deformations by means of a level set method using frequency hopping technique," *IEEE Trans. Antennas Propag.*, **51**, May 2003, pp. 1100–1113.
9. A. Randazzo, "Swarm Optimization Methods in Microwave Imaging," *Int. J. Microw. Sci. Technol.*, **2012**, 2012, pp. 1–12 (491713).
10. T.-J. Cui, W. C. Chew, A. A. Aydiner, and S. Chen, "Inverse scattering of two-dimensional dielectric objects buried in a lossy earth using the distorted Born iterative method," *IEEE Trans. Geosci. Remote Sens.*, **39**, 2001, pp. 339–346.
11. P. M. van den Berg and R. E. Kleinman, "A contrast source inversion method," *Inverse Probl.*, **13**, December 1997, pp. 1607–1620.
12. A. Randazzo, G. Oliveri, A. Massa, and M. Pastorino, "Electromagnetic Inversion with the Multiscaling Inexact Newton Method-Experimental Validation," *Microw. Opt. Technol. Lett.*, **53**, December 2011, pp. 2834–2838.
13. A. Massa, M. Pastorino, and A. Randazzo, "Reconstruction of two-dimensional buried objects by a differential evolution method," *Inverse Probl.*, **20**, December 2004, pp. S135–S150.
14. C. Estatico, M. Pastorino, and A. Randazzo, "An Inexact-Newton Method for Short-Range Microwave Imaging Within the Second-Order Born Approximation," *IEEE Trans. Geosci. Remote Sens.*, **43**, November 2005, pp. 2593–2605.
15. G. Bozza, C. Estatico, M. Pastorino, and A. Randazzo, "An Inexact Newton Method for Microwave Reconstruction of Strong Scatterers," *IEEE Antennas Wirel. Propag. Lett.*, **5**, December 2006, pp. 61–64.
16. C. Estatico, M. Pastorino, and A. Randazzo, "A novel microwave imaging approach based on regularization in Lp Banach spaces," *IEEE Trans. Antennas Propag.*, **60**, July 2012, pp. 3373–3381.
17. C. Estatico, A. Fedeli, M. Pastorino, and A. Randazzo, "Microwave Imaging of Elliptically Shaped Dielectric Cylinders by Means of an Lp Banach-Space Inversion Algorithm," *Meas. Sci. Technol.*, **24**, July 2013, p. 074017.
18. A. Randazzo and C. Estatico, "A regularisation scheme for electromagnetic inverse problems: application to crack detection in civil structures," *Nondestruct. Test. Eval.*, **27**, April 2012, pp. 189–197.
19. J.-M. Geffrin, P. Sabouroux, and C. Eyraud, "Free Space Experimental Scattering Database Continuation: Experimental Set-up and Measurement Precision," *Inverse Probl.*, **21**, December 2005, pp. S117–S130.